Evaluation On Different UAV's Georeferencing Points to Generate Accurate Orthophoto and Digital Terrain Model

*Muhammad Hafiz Aizuddin Mohd Zaidi[1] & Khairul Nizam Tahar[2]**
[1]Dewan Bandaraya Kuala Lumpur (DBKL), Department of Infrastructure Planning, Level 10 North, Menara DBKL 2, Jalan Raja Laut, 50350 Kuala Lumpur, Malaysia
[2]Centre of Studies for Surveying Science and Geomatics, Faculty of Architecture, Planning and Surveying, Universiti Teknologi MARA, 40450 Shah Alam, Selangor, Malaysia.
**Corresponding author: khairul0127@uitm.edu.my*

Received: 15/06/2021
Reviewed: 13/7/2021
Accepted: 30/7/2021

ABSTRACT

UAV or drone application of autonomy ranging can be divided into several levels, from basic hovering and position over trajectory tracking and waypoint navigation to fully autonomous navigation. This study used the DroneDeploy application for an autonomous flight mission. It is the process of taking photographs from an aircraft or other flying objects with a camera mounted on them to produce a three-dimensional (3D) map from the images captured, including a digital terrain model (DTM) and orthophotos. As for this study, the same output will be generated, but different flight parameter applications were used. Therefore, the study determined the optimum number of ground control points (GCPs) and evaluated the accuracy of the final results for each flight design. Acquired data were processed using the Pix4D modeller software due to the user-friendly factor and faster processing rate offered by the software. The results were analysed, and recommendations were made for future study improvement and to avoid similar problems. This study is useful for the mapping industry to achieve high accuracy results.

Keywords: Aerial photogrammetry, Flight Parameter, UAV apps, DTM, Orthophotos, GCPs

INTRODUCTION

An unmanned aerial vehicle (UAV) or a drone is an aircraft without human control aboard. A drone has initially been implemented in military applications. Then, it was developed into commercial, scientific, recreational, agricultural, archaeological and other applications. Drones are commonly used in applications where the operating site cannot be accessed by land vehicles or applications that require an in-flight or airborne view of the selected site (Mohamed et al., 2020; Sun et al., 2018). The UAV flight may operate with various autonomy degrees, either remotely piloted by a human operator or autonomously by onboard computers or mobile applications. The common types of UAV systems are fixed-wing and multi-rotor, which have their benefits and weaknesses. The fixed-wing UAVs, which were once constantly used by the military (e.g., Predator or Global Hawk), are large, expensive and limited autonomy vehicles with special task purposes. Furthermore, according to Sanz-Ablanedo et al. (2018), successful deployment of small UAVs needs a robust and lightweight platform, lightweight autopilot, a low-power, easy-to-use human interfaces, and increased autonomy, including path planning and tracking algorithms.

In terms of benefit, the area coverage of fixed-wing UAVs is larger than the multi-rotor types, whereby the system has limitations due to the battery power storage. As for multi-rotor UAVs, they are easy to fly, have deployment and landing procedures, and perform in an autonomous flight (semi or fully autonomous system). As for the flight functions, UAVs were exploited in civilian and commercial applications. For example, UAV application in precision agriculture involves better management of farm inputs such as fertilisers, fuels, and pesticides. According to Boon (2017), the proper management practice and advanced UAV technology can improve crop production escalation.

UAV systems are also used for emergency mapping, whereby the application provides situational awareness of emergency management and immediate crisis information for the response. In addition, the use of UAV technology in wildlife management has so far been limited to the occasional observation of animal species, such as bison, roe deer, alligator, and marine mammals (Polidori & El Hage, 2020; Giordan et al., 2020; Chen et al., 2020). The application is also used for counts of colony nesting birds.

The main features of UAV photogrammetry are considered concerning costs (low–cost), flight altitude (low–high), and capability of image acquisition in real-time. The quality depends on sensor features, flight performance, atmospheric and environmental conditions, wind influence and other features (de Moraes & de Freitas, 2020). Different UAV types and classifications are applied for photogrammetric data acquisition. UAV photogrammetry data acquisition is possible to be carried out manually, in semi-automated or automated flight mode. The UAV application in recent robotics research studies was varied, especially in the level of autonomy, ranging from basic hovering and position holding over trajectory tracking and waypoint navigation to fully autonomous navigation. The acquired UAV images were processed by specialised software for the photogrammetric survey, such as Agisoft Photoscan, Pix4D and photo mode. Generally, UAVs have two (2) digital aerial image processing methods, which involve the traditional and digital methods, which involve software available in computer (PC) version. In the current advanced technological era, the software method in processing UAV images is preferred because it is easy and saves time (Jouybari et al., 2021; Zhang et al., 2021). However, in the photogrammetric survey, vital aspects before flight missions such as its parameters and ground control point coordinates must be considered to obtain good and accurate results.

The digital elevation model (DEM) contains the elevation of a point on a surface above the mean sea level (MSL). There are various techniques in acquiring the elevation data of DEM creation (e.g., land surveying or remote sensing technology). Still, photogrammetric technology is commonly used, especially with UAVs (Su, 2019). Orthophoto image is also the output of photogrammetric technology, which is defined as a photograph that has been geometrically corrected (orthorectified). Compared to a raw aerial photo, an orthophoto image can be used to measure the true distance due to its accurate Earth's surface representation (Orjales et al., 2021; Sankey et al., 2017). Therefore, this study describes and evaluates the performance of three (3) different flight systems for UAV mapping to find the optimal parameters for producing accurate orthophoto images and digital terrain models (DTM).

This study aims to determine the optimum number of ground control points (GCPs) for flight missions. The study area involved was in a government institutional compound at Universiti Teknologi Mara (UiTM) Shah Alam. It was located at an inclined hill that was suitable for the study purpose. Images were captured using a quadcopter UAV, namely DJI Phantom 4, which was more appropriate for mapping purposes due to a balanced feature of the UAV body structure. The flight parameters were set accordingly, which comprise altitude of flight missions that were set similar, respectively, which was 50 m, seven (7) ground control points (GCPs) and 29 verification points (VPs) for accurate assessment and control. The forward lap (overlap) and side lap were set at 80% and 60%, respectively.

MATERIAL AND METHODS

In this study, the flight parameters were set on-site using the flight application, DroneDeploy. The system is user friendly and simplifies the calculation of GSD and flight time/speed by proposing the default parameter setting as in the introduction. The parameter details involved in this study are shown in Table 1. The sensor parameters set on flight mission involved the Phantom 4 UAV, which was flown at 50 m altitude for every application validated in this study. The flight missions were carried out, in which 7 GCPs were marked on the ground, and each GCP coordinate was recorded using the GPS survey methodology, MyRTKnet technique.

Meanwhile, 29 VPs were marked on the ground. The coordinates were detailed using the conventional survey method, a tacheometry survey since the total VPs were many to be established. Therefore, the tacheometry survey was suitable and more efficient to conduct. The coordination of point locations did not necessarily follow the pre-design plan, which depended on many factors, especially geographic factors. For example, the location was covered by many trees, or the area was not accessible to man. The control points must be seen when the image was captured since it was vital during processing.

Figure 1: DJI Phantom 4 Drone

Table 1: Flight mission parameters arrangement

UAV Type/Brand	DJI Phantom 4 (Quadcopter)
Sensor	Focal Length: 24 mm
Parameter	GSD: 6 cm
Flight	Altitude: 50 m
Parameters	Overlap & Sidelap: 80% and 60%
	Total Distribution: 7 GCPs/ 29 VPs
Control Points	Processing Phase: 4, 5, 6 and 7 GCPs with each flight task include 29 VPs together.

RMSE accuracy analysis will justify the variable of parameters. The workflow of the study components involved is illustrated in Figure 1. The area of study was mainly chosen for its hill slope pattern factor, which was suitable for the accuracy of the terrain pattern study. The area was approximately 4 ha, whereby the GCP and VP distributions were balanced, and it systematically covered the whole area (Figure 2). The flight line was customised, whereby the grid vertices were extended to cover the entire area; the altitude was fixed at 50 m. The different selection number of GCPs in this was referring to the previous study done by Tahar (2013), Jaud et al. (2016) and Oniga et al. (2018), where the ideal number of GCPs depend on the size and shape of the study area. The GCPs configuration also plays an important role to make sure the absolute orientation is well performed. The GCPs configuration should be well distributed within the study area to reduce the seamless line on the final products. Therefore, 4, 5, 6 and 7 GCPs have been used in this study to investigate the effect of orthophoto and digital terrain model products.

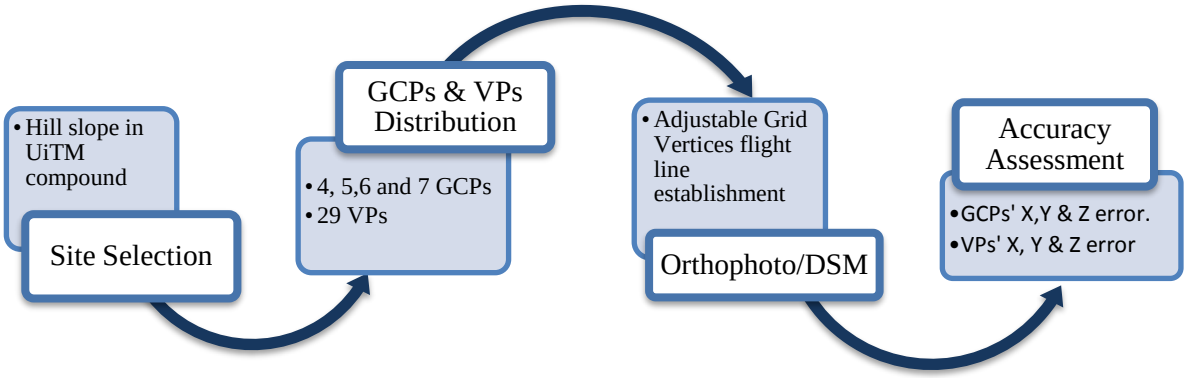

Figure 2: General flowchart of the study

The established GCPs and VPs were based on the pre-design plan (Figure 3) for the location marking. The plan acted as a reference to achieve the required well-distributed points. Methods for obtaining the coordinate points were different for both points, in which for GCPs, the coordinates were acquired from a GPS survey with the MyRTKnet technique. The marking of GCPs was used painted wooden board with the specific design as illustrates in Figure 4.

Figure 3: GCPs and VPs establishment in the study area where the total number is 7 and 29 points.

Figure 4: GCPs establishment; (Left) GCPs board marker and (Right) GCPs marking on the ground using MyRTKnet technique.

The GCPs board can assist during image processing where the identification of GCPs on the image is crucial. The marking should be as sharp as possible to avoid any displacement during image processing. While all VPs have been established using the setting-out survey technique, each point's coordinates have been stored automatically in the total station. The setting-out survey is the reverse of the surveying process. The process involves the positions and levels of building lines and road alignments shown on the construction plans by various techniques and instruments to be established on the ground. In carrying out the survey, the GM-100 series must work with other additional instruments: mini prism, prism, and tripod (Figure 5). After the survey, the coordination of points location does not necessarily follow the pre-design plan. It depends on many factors, mainly geographic factors such as the location is covered by many trees or the area is no man access area. Meanwhile, VPs were established with a setting-out survey technique, and the coordinates were technically obtained after a point was surveyed. After the survey, coordination of the point locations will not necessarily follow the pre-design plan, depending on many factors, especially geographic factors such as if the location is covered by many trees or the area is not accessible.

Figure 5: Topcon GM-100 Series and all the additional instruments (Topcon, 2019)

After all the GCPs and VPs have been marked and recorded, the flight mission can be resumed where the designed flight lines should cover the whole study area, including all GCPs and VPs. The flight mission apps used in this study is known as DroneDeploy. DroneDeploy apps can design normal grid flight patterns, which the flight line is diagonally design and generated (Figure 6). For safety reasons, the coverage of flight lines should be bigger than the study area to make sure the aerial images cover the targeted study area even though there is a slight wind effect during the flight mission. The designed flight lines involve flight parameters such as altitude, sidelap percentage and overlap percentage. Users need to define these desired parameters during flight mission design. In this study, altitude 50 meters, overlap percentage 80% and sidelap percentage 60% has been configured. DroneDeploy apps can determine the GSD value, automatically predicted from the selected flight altitude and camera sensor. Once all flight parameters have been set, then the designed flight lines were sent out to UAV. DroneDeploy has an automatic function to send out the data directly to a connected UAV. These apps also can check all requirements before a UAV execute a flight mission.

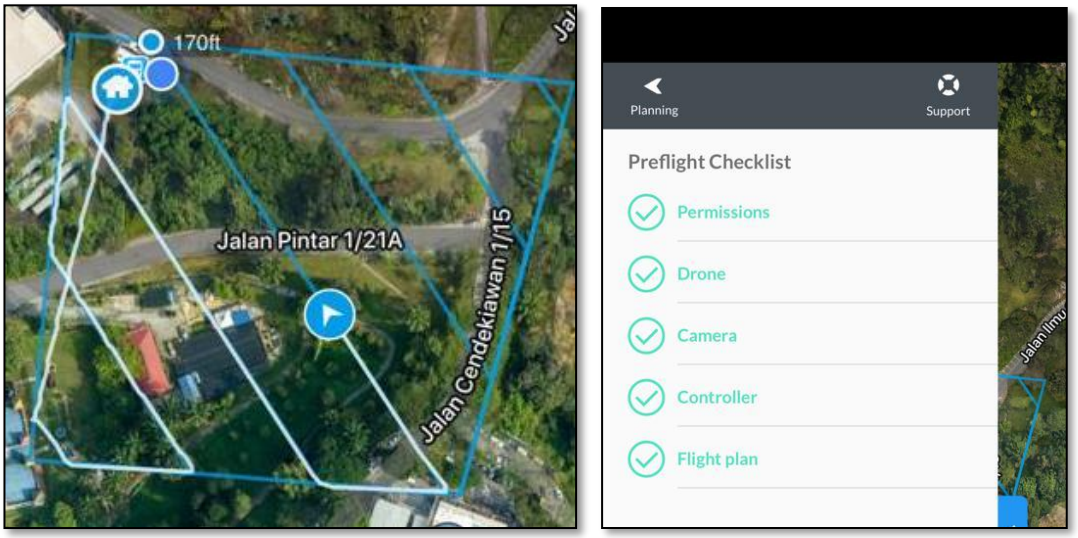

Figure 6: (Left) The flight line of the mission and (Right) Checklist of preflight mission

RESULTS AND ANALYSIS

The result covered the accuracy of checkpoints from orthophoto products based on the number of GCP distributions (during processing). The results of X, Y and Z errors and RMSE for each different number of GCPs and VPs distribution are shown. Figure 7 shows the result of end products generated, orthophoto and digital surface model (DSM) of the study area.

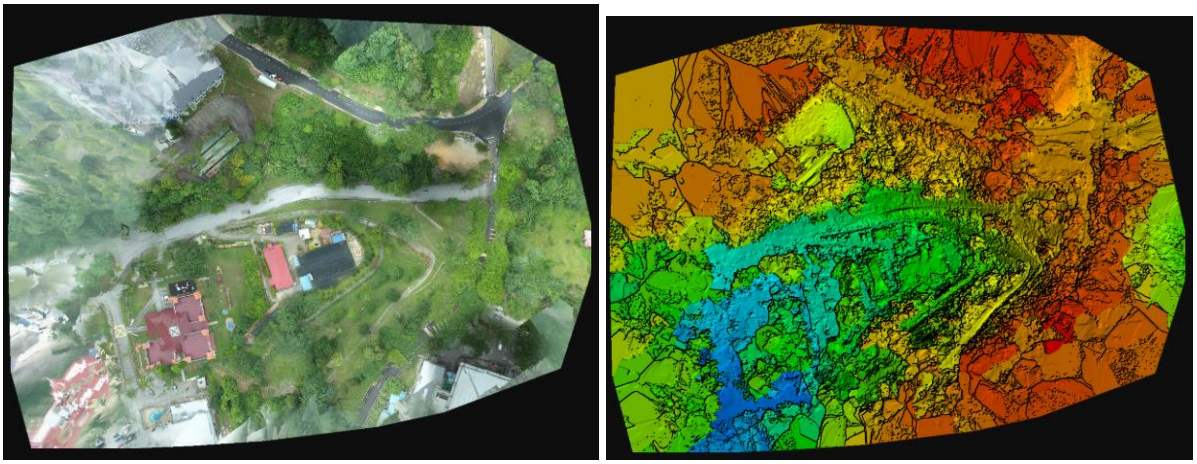

Figure 7: Final products of processing

Table 2: RMSE value of VPs of 4 and 5 GCPs distribution

Points	4 GCPs			5 GCPs		
	X (m)	Y (m)	Z (m)	X (m)	Y (m)	Z (m)
VP7	0.230	-0.099	-2.550	0.305	-0.108	-2.765
VP8	0.125	-0.106	-2.538	0.202	-0.100	-2.818
VP13	0.044	1.197	-2.587	0.060	1.160	-2.630
VP14	0.929	0.184	-1.563	0.946	0.146	-1.611
VP15	0.742	0.421	-1.130	0.760	0.384	-1.185
VP16	-0.104	0.355	0.176	-0.081	0.320	0.111
VP17	0.108	0.033	0.287	0.130	-0.001	0.207
VP19	0.393	0.044	-0.866	0.418	0.012	-0.949
VP21	0.062	0.061	-2.246	0.089	0.028	-2.342
VP22	0.504	0.162	-2.155	0.533	0.126	-2.247
VP25	-0.389	0.951	-3.635	-0.354	0.913	-3.732
VP27	0.707	0.298	0.160	0.754	0.264	0.036
VP29	0.026	-0.332	-1.078	0.079	-0.363	-1.215
VP30	0.030	0.370	-1.096	0.085	0.344	-1.233
VP31	0.243	0.069	-1.103	0.286	0.037	-1.189
VP32	-0.203	-0.027	-1.104	-0.163	-0.056	-1.179
VP33	0.368	0.064	-1.070	0.406	0.035	-1.137
VP34	0.002	0.051	-1.063	0.038	0.023	-1.118
VP35	-0.321	-0.044	-1.069	-0.288	-0.072	-1.117
VP36	0.201	-0.086	-1.120	0.232	-0.114	-1.154
VP37	-0.171	0.138	-1.125	-0.142	0.112	-1.150
VP38	1.002	0.502	-1.297	1.051	0.469	-1.425
VP39	0.697	0.608	-1.216	0.746	0.574	-1.350
VP43	0.088	0.883	-1.550	0.094	0.870	-1.505
VP44	0.396	0.213	-1.503	0.406	0.191	-1.480
VP45	0.830	0.358	-1.423	0.844	0.323	-1.422
VP46	-0.058	0.529	-5.643	-0.025	0.490	-5.741
VP47	-0.208	0.325	-6.265	-0.177	0.287	-6.360
VP50	0.092	-0.160	-1.337	0.114	-0.195	-1.398
RMSE (m)	0.431	0.419	2.202	0.448	0.400	2.273

Table 3: RMSE value of VPs of 6 and 7 GCPs distribution

Points	4 GCPs			5 GCPs		
	X (m)	Y (m)	Z (m)	X (m)	Y (m)	Z (m)
VP7	0.193	-0.078	-2.548	0.194	-0.085	-2.581
VP8	0.092	-0.092	-2.554	0.092	-0.098	-2.581
VP13	0.049	1.218	-2.567	0.051	1.216	-2.594
VP14	0.933	0.203	-1.543	0.935	0.202	-1.573
VP15	0.743	0.439	-1.113	0.744	0.437	-1.147
VP16	-0.107	0.369	0.193	-0.105	0.368	0.154
VP17	0.102	0.047	0.297	0.105	0.046	0.258
VP19	0.388	0.056	-0.851	0.390	0.056	-0.900
VP21	0.056	0.073	-2.236	0.057	0.072	-2.285
VP22	0.496	0.173	-2.147	0.497	0.172	-2.199
VP25	-0.400	0.956	-3.626	-0.401	0.957	-3.674
VP27	0.694	0.290	0.157	0.685	0.287	0.123
VP29	0.010	-0.344	-1.083	-0.001	-0.350	-1.111
VP30	0.014	0.356	-1.102	0.002	0.349	-1.124
VP31	0.232	0.054	-1.101	0.222	0.048	-1.127
VP32	-0.213	-0.042	-1.099	-0.222	-0.048	-1.127
VP33	0.361	0.048	-1.063	0.351	0.041	-1.090
VP34	-0.005	0.034	-1.055	-0.014	0.027	-1.081
VP35	-0.326	-0.062	-1.060	-0.336	-0.068	-1.087
VP36	0.196	-0.105	-1.111	0.186	-0.111	-1.136
VP37	-0.176	0.117	-1.116	-0.186	0.110	-1.138
VP38	0.988	0.492	-1.300	0.978	0.488	-1.331
VP39	0.683	0.600	-1.222	0.673	0.598	-1.255
VP43	0.100	0.883	-1.520	0.097	0.877	-1.548
VP44	0.404	0.217	-1.478	0.405	0.211	-1.514
VP45	0.835	0.364	-1.403	0.838	0.358	-1.440
VP46	-0.071	0.536	-5.633	-0.073	0.535	-5.684
VP47	-0.219	0.333	-6.255	-0.219	0.333	-6.307
VP50	0.089	-0.148	-1.322	0.091	-0.149	-1.363
RMSE (m)	0.428	0.422	2.195	0.427	0.421	2.225

All checkpoints were processed in Pix4D software, and a report on the result was generated. From the report, each point was computed, and the error was displayed in a table. Each point error was divided into three (3) parts: X, Y and Z errors, and RMSE of all the VPs for each number of GCPs. Each error will be analysed separately for all checkpoints. A line chart of X, Y and Z error coordinates of VPs were generated for the accuracy analysis at different GCP distribution numbers. Figure 8 (a,b,c) shows the X, Y and Z errors, respectively, for all 29 VPs involved. Each flight mission with different GCP numbers had different X error outcomes. The X errors are presented in a line graph of different GCPs.

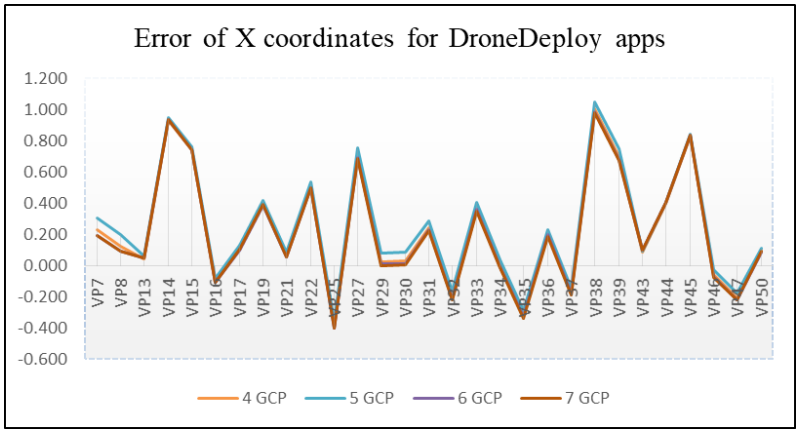

(a)

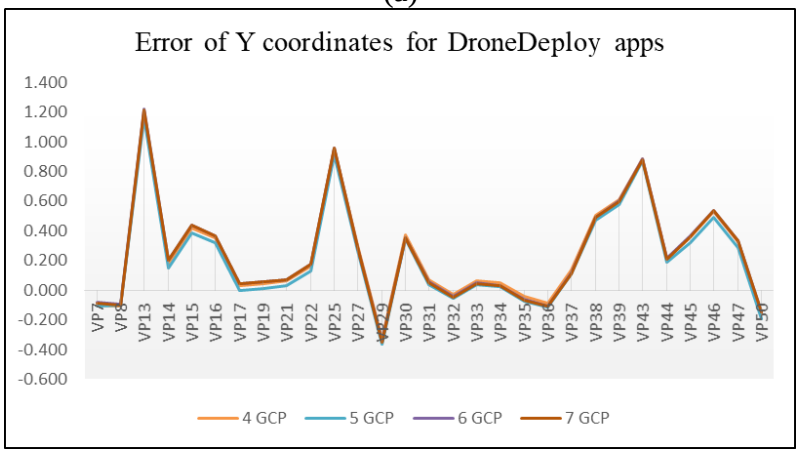

(b)

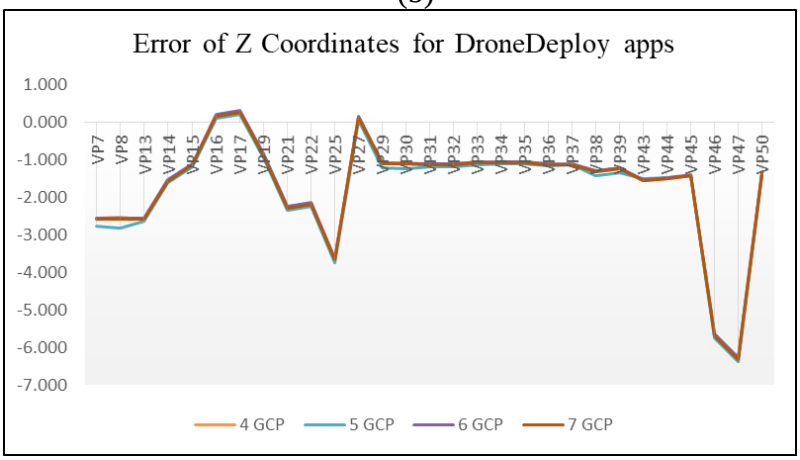

(c)

Figure 8: Error of VPs coordinates graph of all GCPs distribution; a) X coordinates, b) Y coordinates, c) Z coordinates

In Figure 8(a), the X errors all 29 VPs were involved in the DroneDeploy flight mission. Each flight mission, with a different number of GCPs, had different X error outcomes. Amongst the four GCP missions, 7 GCP points had the lowest X error as compared to others. As shown in Figure 8(a), VP_{25} with a value of error at -0.401 m is the lowest value of all VP errors. For the highest X error, 7 GCP points have the highest value, which is 1.051 m. At $VP_{38,}$ the error is high due to the error in marking during processing. Figure 4.20 also shows that the line pattern of each error is similar but with different values of error for each point. The same VP point had the same error for every different number of GCPs. However, the VPs in 7 GCPs flight missions had almost low values compared to other GCPs numbers. It can be concluded that several VP points were not accurately marked because the point was

wrongly identified, and thus it affected the error of coordinate geolocations. The point marked in the software was not the same points as that marked on the field. Therefore, the coordinates were not the same, and a high error was computed.

Figure 8(b) shows the Y error coordinates, whereby all 29 VPs were involved in the DroneDeploy flight missions. Each flight mission with a different number of GCPs had different Y error outcomes. The errors are presented in a line graph of different GCPs. Referring to Figure 8(b), the 6 GCPs flight missions have the highest error compared to other GCP numbers. The highest Y error value was at VP_{13} of 6 GCPs with a value of 1.218 m.

Meanwhile, the lowest value was -0.363 at VP29 of 5 GCPs. Similar to the X error, the line pattern of Y error for every GCPs mission was similar but with different error values. In the graph presented, VP_{25} and VP_{43} almost reached the high error behind VP_{13}. Same as the X error, the line pattern of Y error for every GCPs mission was similar with only different values.

As for Z error of coordinates, all 29 VPs involved in the DroneDeploy flight missions are shown in Figure 8(c). Each flight mission with different GCP numbers had different Z error outcomes. The errors are presented in a line graph of different GCPs, verified as 4 GCPs, 5 GCPs, 6 GCPs and 7 GCPs. Figure 8(c) shows that the 6 GCPs and 7 GCPs flight missions had the lowest error compared to other GCPs numbers. The lowest value was -6.360 m at VP_{47} of 7 GCPs. The highest value of Z error was at VP_{17}, with the value of 0.297 m of 6 GCPs flight missions. The pattern of the line graph in Figure 8(c) was similar between each GCPs mission and thus, showed that the same VP points had produced the same error for every flight mission.

Figure 9 shows the RMSE values of each GCPs and is divided into every error parameter. Each RMSE error was aligned with the total number of 4 GCPs, 5 GCPs, 6 GCPs and 7 GCPs distribution, respectively. The lowest value for X error was with 7 GCPs distribution, which was less 0.001 m than the 6 GCPs distribution. The highest value error was when 5 GCPs distribution was implied with a 0.448 m error value. Y Error coordinates were also analysed, whereby the lowest value of error obtained resulted from 5 GCPs distribution, which was 0.400m.

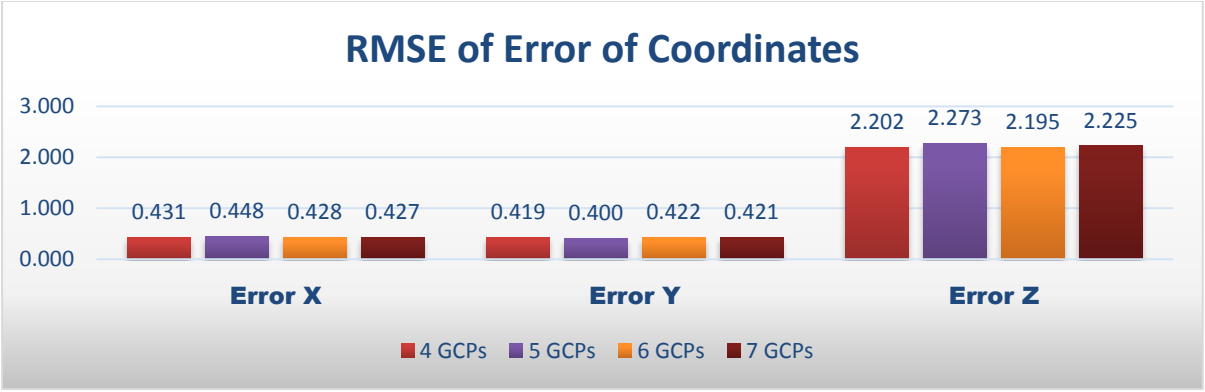

Figure 9: The RMSE of X, Y and Z coordinates are represented

The difference between the lowest and highest Y error was 0.022m, which concluded that the 6 GCPs distribution had a 0.422 m error value. Finally, the Z error coordinates had the highest error as compared to X and Y errors. The highest error value resulted from the 5 GCPs distribution with 2.273 m error value compared to the lowest with 2.195 m error value, which was 6 GCPs distribution. The difference of 0.007 m with the lowest value was 4 GCPs distribution with 2.202 m value, while 7 GCPs distribution had a big gap of 0.048 m error value with the highest error value of 2.225 m. Based on RMSE results, it can conclude that the 6 and 7 GCPs have shown consistent accuracy in X, Y and Z coordinates. However, the different accuracy between 4,5,6 and 7 GCPs is not much different. The advanced analysis using ANOVA statistics has been performed to analyse which GCPs configuration is the best. Table 4 illustrates the standard error of X coordinates for all numbers of GCPs less than F-

stat, standard error of Y coordinates more than F-stat for all number of GCPs, and standard error of Z also coordinates beyond than F-stat. However, the P-value shows good results for X, Y and Z coordinates.

Table 4: ANOVA Statistic Summary

	Mean	Std. Dev.	Std. Error	F-Stat	P-value
			X coordinates		
4GCPs	0.220	0.377	0.070	0.087	0.967
5GCPs	0.253	0.377	0.070		
6GCPs	0.212	0.379	0.070		
7GCPs	0.208	0.379	0.070		
			Y coordinates		
4GCPs	0.240	0.350	0.065	0.051	0.985
5GCPs	0.210	0.347	0.064		
6GCPs	0.241	0.353	0.066		
7GCPs	0.237	0.354	0.066		
			Z coordinates		
4GCPs	-1.680	1.449	0.269	0.023	0.995
5GCPs	-1.762	1.462	0.271		
6GCPs	-1.671	1.449	0.269		
7GCPs	-1.706	1.454	0.270		

Based on Table 4, summarise that the standard error for all GCPs with respect to X, Y and Z coordinates is not significant in this study area. The optimum number of 4 GCPs can be used in this study area because it gives high accuracy data. Nevertheless, the configuration of GCPs should be well distributed all over the study area to achieve high accuracy results.

CONCLUSION AND FUTURE WORK

In conclusion, most results that had the lowest RMSE error was 7 GCPs distribution. It can be said that the number of GCPs and checkpoints or VPs are important in accessing better accuracy. Not to mention, the GCPs and VPs involved must be well distributed in the study area to get high-quality orthomosaic images. Based on the results, the orthophoto of 7 GCPs produced better presentation quality than the other number of GCPs. Based on the RMSE, it can be concluded that the 5 GCPs distribution have the highest error for error X and error Z, while error Y was the lowest. As for the optimum number of GCPs distribution, 7 GCPs had the best result because of the lowest value of error X, and consistent value of error Y and error Z. 5 GCPs and 7 GCPs distributions both had well-distributed control points as compared to 4 GCPs and 6 GCPs distributions, in which the difference was that the 5 GCPs and 7 GCPs distributions had covered the whole area and centre. However, since the numbers of GCPs were not equally balanced in terms of accuracy coverage, the results may be the lowest or highest because of the unbalanced factor. As compared to 4 GCPs and 6 GCPs distributions, the number and distributions were equally balanced. Thus, the result accuracy will be the lowest or a consistent value, preferable to the high error values. Nevertheless, all error values were acceptable since the values were lower than 1 of tolerance.

Further research is necessary to determine suitable methods to generate more precise orthophotos and DSM of model. The study included flight parameters from multiple altitude image captures to combine large and mini scales of an area. Since the higher number of overlapping images could produce more DTM triangulation structures, it provides highly accurate orthophotos and DSMs, whereby accuracy assessments could also be carried out. Moreover, future researchers can establish more GCP and VP numbers. It must be systematically designed to cover the whole study area with a well distribution design. The higher the control points and well distributed, the higher the accuracy of the processing end products, which in this case, accurate orthophotos and DSMs were generated.

ACKNOWLEDGEMENT

Faculty of Architecture, Planning, and Surveying Universiti Teknologi MARA (UiTM), Research Management Institute (RMI) and Ministry of Higher Education (MOHE) are greatly acknowledged forproviding the fund GPK Grant number 600-RMC/GPK 5/3 (223/2020) to enable this researchto be carried out. The authors would also like to thank the people who were directly or indirectly involved in this research.

REFERENCES

Boon, A. P. (2017). Comparison Of A Fixed-Wing And Multi-Rotor Uav For Environmental Mapping Applications: A Case Study. The International Archives of the Photogrammetry, Remote Sensing and Spatial Information Sciences, 47-54

Chen, P.F., & Xu, X.G.(2020). A comparison of photogrammetric software packages for mosaicking unmanned aerial vehicle (UAV) images in agricultural application. Acta Agron. Sin. 2020, 46, 1112–1119.

de Moraes, R.S., & de Freitas, E.P. (2020). Multi-UAV Based Crowd Monitoring System. *IEEE Transactions on Aerospace and Electronic Systems*, vol. 56, no. 2, pp. 1332-1345, April 2020, doi: 10.1109/TAES.2019.2952420.

Giordan, D., Adams, M.S., Aicardi, I. et al. (2020). The use of unmanned aerial vehicles (UAVs) for engineering geology applications. Bull Eng Geol Environ 79, 3437–3481 (2020). https://doi.org/10.1007/s10064-020-01766-2

Jaud, M., Passot, S., Le Bivic, R., Delacourt, C., Grandjean, P., & Le Dantec, N. (2016). Assessing the Accuracy of High-Resolution Digital Surface Models Computed by PhotoScanR and MicMacR in Sub-Optimal Survey Conditions. Remote Sens. 2016, 8, 1–18.

Jouybari, A., Bagherbandi, M. & Nilfouroushan, F. (2021). Comparison of the strip- and block-wise aerial triangulation using different exterior orientation parameters weights, Journal of Spatial Science, DOI: 10.1080/14498596.2020.1871086

Mohamed, E.A., Albert, Y.G., & Amr, E.M. (2020). Improving the Accuracy of RTK-GNSS Data in Digital Elevation Model. ICGDA 2020: Proceedings of the 2020 3rd International Conference on Geoinformatics and Data AnalysisApril 2020 Pages 86–90https://doi.org/10.1145/3397056.3397071

Oniga, V.E., Breaban, A.I. & Statescu, F. (2018). Determining the Optimum Number of Ground Control Points for Obtaining High Precision Results Based on UAS Images. Proceedings 2018, 2, 352, doi:10.3390/ecrs-2-05165

Orjales,F.;Losada-Pita,J.; Paz-Lopez, A.; Deibe, Á. (2021). Towards Precise Positioning and Movement of UAVs for Near-Wall Tasks in GNSS-Denied Environments. Sensors 2021, 21, 2194. https://doi.org/ 10.3390/s21062194

Polidori, L., & El Hage, M. (2020). Digital Elevation Model Quality Assessment Methods: A Critical Review. *Remote Sens.* 2020, *12*, 3522. https://doi.org/10.3390/rs12213522

Sankey, T., Donager, J., McVay, J., & Sankey, J.B. (2017). UAV lidar and hyperspectral fusion for forest monitoring in the Southwestern USA. Remote Sens Environ 195:30–43. https://doi.org/10.1016/j.rse.2017.04.007

Sanz-Ablanedo, E., Chandler, J. H., Rodríguez-Pérez, J. R., & Ordóñez, C. (2018). Accuracy of Unmanned Aerial Vehicle (UAV) and SfM photogrammetry survey as a function of the number and location of ground control points used. *Remote Sensing*, *10*(10). https://doi.org/10.3390/rs10101606

Su, R.D. (2019). Application of UAV in modern agriculture. Jiangsu Agric. Sci. 2019, 47, 75–79.

Sun, G., Huang, W.J., Chen, P.F., Gao, S. & Wang, X. (2018). Advances in UAV-based Multispectral Remote Sensing Applications. Trans. Chin. Soc. Agric. Mach. 2018, 49, 1–17.

Tahar, K.N. (2013). An Evaluation On Different Number Of Ground Control Points In Unmanned Aerial Vehicle Photogrammetric Block. *International Archives of the Photogrammetry, Remote Sensing and Spatial Information Sciences, Volume XL-2/W2, ISPRS 8th 3DGeoInfo Conference & WG II/2 Workshop, 27 – 29 November 2013, Istanbul,Turkey*, *XL*(November), 27–29.

Topcon, (2019). *The Future is Now*. Retrieved from Topcon Positioning: https://www.topconpositioning.com/

Zhang, H., Wang, L., Tian, T. & Yin, J. (2021). A Review of Unmanned Aerial Vehicle Low-Altitude Remote Sensing (UAV-LARS) Use in Agricultural Monitoring in China. Remote Sens. 2021, 13, 1221. https://doi.org/10.3390/rs13061221